

Time correlated fluorescence characterization of an asymmetrically focused flow in a microfluidic device

Silvia Carlotto · Ilaria Fortunati · Camilla Ferrante ·
Petra Schwille · Antonino Polimeno

Received: 28 May 2010 / Accepted: 28 June 2010 / Published online: 14 September 2010
© Springer-Verlag 2010

Abstract In this study, we explore and model the behavior of a prototype microfluidic device which employs two non-mixing fluids (sheath and inlet fluids) displaying an asymmetric focused flow, in the presence of a fluorescent dye. Fluorescence correlation spectroscopy is employed, allowing the precise measure of flow speeds across the channels and of the concentration profile of the central focused flux along the flow direction. The system is modeled via a standard Navier–Stokes finite-element approach, coupled to convection–diffusion equations for the solute. Simulations reproduce accurately the shape, the position, and the width of the velocity and concentration profiles along the central channel and across the transversal and vertical sections of the microfluidic device. The observed asymmetric flow with respect to the center of the channel is reproduced numerically with an error in the position determination smaller than 1%.

Keywords Microfluidics · Hydrodynamic focusing · Fluorescence correlation spectroscopy · Navier–Stokes equations

1 Introduction

In the last decade, microfluidic devices have emerged as a new and exciting route to explore miniaturization of chemical synthetic procedures, with enormous benefits such as reduced size, improved performance, low cost, reduced sample, and reagent volume (Mark et al. 2010). The small size of microchannels leads to a small Reynolds number and a stable laminar flow (Brody et al. 1996). The flow dynamics is therefore easily predictable, allowing a careful control of the conditions under which bio-chemical reactions can be carried out.

In this article, we address a joint experimental and numerical investigation of an essential device exploiting the ‘hydrodynamic focusing’ effect, which is a relatively simple but powerful method for handling a sample stream. Our interest lays mainly in a detailed comparison between experimental data and the prediction of numerical simulations, in order to test the usefulness of the latter in the design of simple microfluidic devices for specific applications.

The simplest device for hydrodynamic focusing consists of three inlet channels (Wu and Nguyen 2005), i.e., a cross-like geometry with the focusing sheath fluid channels perpendicular to the main sample channel in which detection is performed. Several studies explore the influence of the side channels geometry (Simonnet and Groisman 2005; Chang et al. 2007) and the effect of small (Wu and Nguyen 2005), modest (Larsen and Shapley 2007) and large (Cubaud and Mason 2008) viscosity difference among the fluids on the width of the central stream.

The basic idea is derived from conventional flow cytometry (Lee et al. 2001a; Yang and Hsieh 2007; Chung et al. 2003). Flow cytometry in general (Ghosh et al. 2008; Srisa-Art et al. 2009), and hydrodynamic focusing methods

S. Carlotto · I. Fortunati · C. Ferrante (✉) · A. Polimeno (✉)
Dipartimento di Scienze Chimiche e UdR INSTM, Università
degli Studi di Padova, Via Marzolo 1, 35131 Padova, Italy
e-mail: camilla.ferrante@unipd.it

A. Polimeno
e-mail: antonino.polimeno@unipd.it

P. Schwille
Biotechnologisches Zentrum (BIOTEC), Technische Universität
Dresden, Dresden, Germany

in particular, are efficient techniques to divide, count, or even sort microparticles or different cell subpopulations (Liu et al. 2009; Chen et al. 2009). Cells and microparticles manipulation and separation is an essential requirement in many biological (Lin et al. 2008) and analytical applications. Cells/microparticles can be focused into a narrow sample stream and they are then driven through the region of interest where they are recognized and traced in real time. Sorting of micro-objects like particles or living cells by selective separation based on size or other feature can be implemented using magnetic force (Pamme and Wilhelm 2006), electrophoresis (Kohlheyer et al. 2006) or hydrodynamic principles (Yamada and Seki 2006) on focused stream. The underlying principle common to these applications is that a force acts on suspended micro-objects while the liquid stream remains more or less unaffected (Mark et al. 2010). Other cytometric applications for focused flows are in the area of disease monitoring (Fenili and Pirovano 1998), cell biology (Wang et al. 2008), immunotoxicology (Criswell et al. 1998), DNA sizing (Wong et al. 2003) and quantitative analysis of white blood cells (Kim et al. 1998).

A completely different application of the focusing effect exploits the very smooth and relatively stable interface between different liquids in a microchannel under laminar flow conditions. This feature allows for the generation of optical micro-components, such as waveguides, lenses, and mirrors. Song et al. (2009) showed the possibility of obtaining fluidic microlenses with different curvatures by manipulating the flow rates of three streams in a circular chamber. Changing the ratio of the lateral stream velocities leads to the generation of negative or positive lenses with different focal lengths.

A significant feature in laminar flows is the poor mixing efficiency. When microfluidic devices are used as microreactors, it is necessary to enhance mixing among the species that are injected in the channels through a cross-junction. Many different strategies have been explored to enhance mixing; one of the simplest, proposed by Hertzog (2006), relies on the insertion of a bottleneck in the central channel, just after the cross-junction between central and sheath fluids. The enhancement of the mixing caused by the bottleneck is measured as a reduction of the mixing time. In general, the reduction of the focused stream facilitates the diffusion-controlled mixing processes (Zhang et al. 2008).

To experimentally test the flow characteristics in a microfluidic device, it is necessary to use appropriate techniques. Recently, fluorescence correlation spectroscopy (FCS) has been used to characterize parameters such as concentration and velocity field profiles in microchannels. FCS is an efficient analytical tool for studying concentrations, diffusion dynamics, interactions, and laminar

flow of molecules at nanomolar concentrations. In FCS, the light emitted by a fluorescent tracer is measured when it streams through a diffraction-limited volume element. The extremely small dimensions of the excitation volume of the order of 1 fl or less (typically volumes range from 1 to 0.1 μm^3 depending on the microscope objective) permit high spatial resolution in the optical detection, making the method ideal for the characterization of micro- and nanostructures (Brister et al. 2005). By scanning the focus of the microscope lens across a microchannel, local parameters such as fluid concentrations and velocities can be measured with an average spatial resolution of 200 nm in the focal plane and down to 1 μm in the axial plane, making it possible to get accurate three-dimensional maps of a microfluidic device (Kuricheti et al. 2004a; Gosch et al. 2000; Dittrich and Schwille 2002). The excellent sensitivity towards low concentrations in the limit of single-molecule detection is another important benefit for the characterization of microfluidic devices where the injected fluid volume is tiny. FCS allows therefore assay miniaturization without compromising the detection sensitivity, making it an ad-hoc analytical method for integration of assays into highly efficient microfluidic platforms. FCS was employed to probe fluids behavior after their manipulation in microchannels especially for mixing and sorting (Yeh et al. 2006; Dittrich and Schwille 2003). Recently, other methods were employed for the characterization of hydrodynamic focusing, such as the micro-PIV (Domagalski et al. 2007) and the voltammetric analysis (Deshpande et al. 2009). Micro-PIV is a wide spread and powerful technique for the characterization of flow velocity in microfluidic devices especially at very low flow rates of the order of 500 $\mu\text{m s}^{-1}$, as demonstrated by many reviews in the field (Sinton 2004; Wereley and Meinhart 2010). The major limitations of the PIV technique are related to the use of large particle tracers, especially for application in nanofluidics, and relatively low spatial resolutions when particles larger than 300 nm are used. The second method employs an electrolyte solution and an electrode. The limiting step results from the necessity of an efficient transport of the electroactive reagent to the electrode surface, especially at high throughput rates. To overcome this problem, further engineering the channel and the electrode could be the way to minimize the total amount of reagents and optimize the throughput sample.

Experimental evidences can be analyzed using numerical models. Treatments of hydrodynamic focusing have been developed for 2D hydrodynamic focusing in a cross configuration (Lee et al. 2001b; 2006), (Nguyen and Huang 2005) and 2½ D focusing (Darnton et al. 2001; Xuan and Li 2005), based on the Navier–Stokes equation in the limit of low Reynolds number. Numerical simulations of microchip focusing were discussed by Ren et al. (2003) and Nguyen

et al. (2008), who obtained the viscosity and the stress tensor of the sample stream by measuring the width of the central stream using a prediction algorithm that uses the channel geometry, the fluid properties and flow rates. All these numerical models and simulations consider perfectly symmetric flux conditions between the two lateral channels and focus their attention mainly on the width of the central flow (Wang et al. 2008). Lee et al. (2006) showed an asymmetric hydrodynamic focusing device in a two-dimensional model applied to polystyrene microparticles, while Domagalski et al. (2007) reproduced the asymmetric flux in a simple cross (squared section) centering their attention on the sheet curvature along the plane normal to the flux direction.

In this work, we investigate a simple device with a cross-like junction between pressure-driven central and lateral channels with a common inlet; a bottleneck is inserted just after the junction to investigate its influence on focusing and mixing. The experimental characterization of the device is carried out with the FCS technique. The device displays an asymmetric focused flow, that is precisely reproduced by the numerical simulations, reporting a thorough investigation of a prototype microfluidic device through simultaneous usage of advanced experimental techniques and careful numerical modeling (Park et al. 2006; Egawa et al. 2009).

This article is organized as follows. Section 2 describes the FCS measurements set-up, device fabrication, and the FCS data analysis for flow and concentration measurements. Next, Sect. 3 is dedicated to numerical simulations of the system. Finally, Sect. 4 is provided on the comparison between the experimental data and computational results.

2 Experimental

2.1 FCS measurements set-up

FCS was performed on a commercial system consisting of an inverted Confocal Laser Scanning Microscope (CLSM; Mod. LSM510, Zeiss, Jena, Germany) and a ConfoCor3 system (Zeiss, Jena, Germany). The exciting laser source was the line at 488 nm of an Ar laser attenuated by an acousto-optical tunable filter to suitably reduce the output power. The laser was directed via a 488/633 dichroic mirror onto the back aperture of a Zeiss C-Apochromat 40X, N.A. = 1.2, water immersion objective. This objective is equipped with a specialized correction collar that changes the spacing between central lens groups inside the objective barrel. For every measurement, the correction collar was adjusted to compensate for the subtle differences in the coverglass thickness (in the range 130–210 μm) and ensure optimum objective performance and fluorescence collection efficiency.

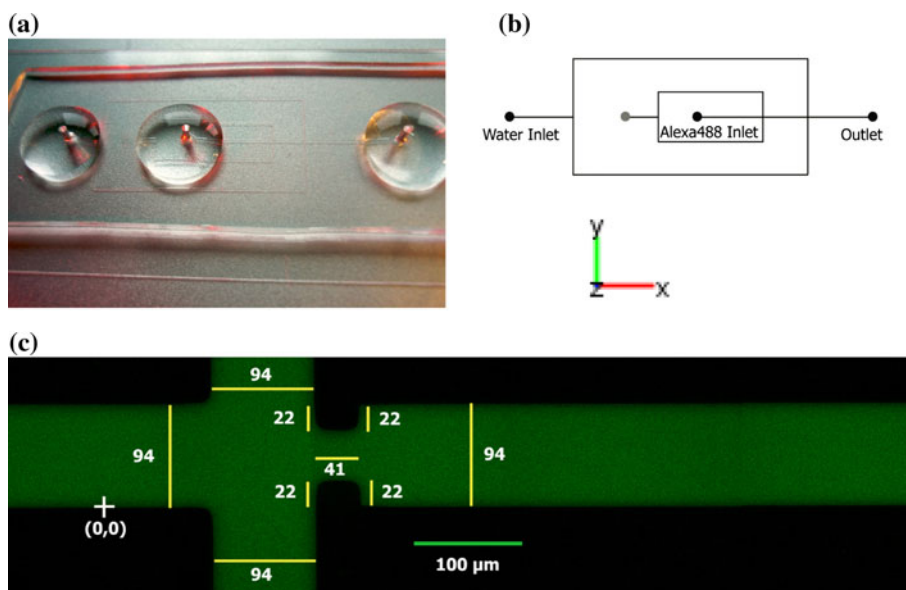
Fluorescence emission was collected by the same objective and split into two parts by a 50/50 beam splitter and sent to two avalanche photodiodes (APDs) used as detectors. To remove any residual laser stray light, two 505-nm longpass filter were inserted in front of the APDs. Out-of-plane fluorescence was reduced with a 70- μm pinhole. The pinhole alignment at the ConfoCor3 was routinely checked at the beginning of each measurement series. The lateral positioning (x,y) is checked with a quick subroutine in the Zeiss software, by translating the pinhole and determining the position of highest fluorescence signal. The axial position (z) of the pinhole is not adjustable with the ConfoCor3-device. However, the lens collimating the divergent excitation beam, when entering into the laser scan head (collimator lens), can be axially (z) moved by the software, and the position of the collimator lens yielding the highest fluorescence signal was chosen. At first, the CLSM image at half-depth of the microchannel was collected. Then by selecting the point-mode configuration, the excitation laser beam was focused in a marked site across the microchannel for further FCS measurement.

The collected fluorescence signals were software-correlated and the FCS curve was evaluated with OriginPro 8 by using Levenberg–Marquardt nonlinear least-square fitting algorithm.

2.2 Device fabrication

The microfluidic device was prepared by replica molding in PDMS (Sylgard 184, Dow Corning, MI) of a patterned SU8 master. After the thermal polymerization, the 1 mm thick PDMS layer was peeled from the master and exposed to reactive oxygen plasma to permit further sticking to a coverglass. The structure of the final microdevice is depicted in Fig. 1a–b. The holes on the left side are used as two inlets for the central and sheath fluids, respectively, and the one on the right is the outlet. The laser beam is focused inside the channel from the coverglass back side. The internal dimensions of the rectangular channels were determined looking at the fluorescence images collected with the CLSM and the APD detector. To this end, the channels were filled with a water solution of the fluorescent dye Alexa488 (Molecular Probes) excited by the 488 nm line of the Ar ion laser. Figure 1c shows the confocal image reproducing the section in the xy -plane of the geometry used in this hydrodynamic focusing study. The lateral dimensions are indicated in the image. The channel depth, equal to $33 \pm 2 \mu\text{m}$, was obtained from 3D reconstruction of optical sections in the xy -plane collected every 1 μm going from the coverglass to the upper wall in PDMS. The uncertainty on the x,y dimensions is about 2%.

Fig. 1 a–b Geometrical description of the experimental device. **c** CLSM image of the part of the circuit used for testing the hydrodynamic focusing effect. All the dimensions are expressed in μm



2.3 Flow measurements

A 60 nM deionized water solution of pure Alexa488 was used for the flow measurements with FCS technique. A syringe pump (Mod. ceDOSYS SP-4, Cetoni GmbH, Germany) was employed to inject the solution into the microchannels, through LDPE tubing (0.58 mm internal diameter) connected to the inlets of the chip. The flow rates were varied between 0.01 and 30 $\mu\text{l}/\text{min}$.

For the hydrodynamic focusing experiments, the Alexa488 solution and water were injected into the central and the side channels, respectively. The ratio between the side and the central flow speeds was changed by setting different flow rates at the two channel inlets.

3 Data analysis

3.1 FCS data analysis for flow measurements

Fluorescence correlation spectroscopy is based on the analysis of fluctuations of fluorescence intensity of individual molecules in a very tiny volume, defined by a highly focused laser beam through a high numerical aperture microscope objective (Elson and Magde 1974; Lakowicz 2006; Petrov and Schwille 2008). For a single free diffusing molecular species in a fluid, the fluorescence fluctuations are due to the transient passage of molecules in and out the excitation volume, with a characteristic diffusion time scale. Fluorescence fluctuations depend on the properties of the tracer and the optical set-up. In this case, the normalized autocorrelation curve $G(\tau)$ of the fluorescence intensity can be expressed by the following relation:

$$G_{\text{DIFF}}(\tau) = \frac{1}{N} \left(1 + \frac{\tau}{\tau_{\text{DIFF}}} \right)^{-1} \left(1 + \frac{\tau}{S^2 \tau_{\text{DIFF}}} \right)^{-1/2} \quad (1)$$

In this expression, τ is the lag time, N is the average number of molecules in the detection volume, $\tau_{\text{DIFF}} = \omega_0^2/4D$ is the time associated with diffusion, and D is the diffusion coefficient. S is the confocal shape factor, i.e., the ratio between the axial (z_0) and the lateral (ω_0) radius at which the Gaussian laser beam profiles decrease to e^{-2} of its maximal intensity.

For most organic fluorophores, the fluorescence brightness is not constant. One of the most common processes affecting it is the transition to the triplet state by intersystem crossing. In this case, the fluorophore remains dark until the transition from the triplet to the ground state takes place (Lakowicz 2006). As a result, the autocorrelation curve in the timescale of the triplet state lifetime (up to 10–20 μs) is influenced by this process and the correct expression for $G(\tau)$ is modified to take into account this second process:

$$\begin{aligned} G(\tau) &= G_{\text{DIFF}}(\tau) \cdot G_{\text{TRIPLET}}(\tau) \\ &= \frac{1}{N} \left(1 + \frac{\tau}{\tau_{\text{DIFF}}} \right)^{-1} \left(1 + \frac{\tau}{S^2 \tau_{\text{DIFF}}} \right)^{-1/2} \\ &\quad \times \left[1 + \frac{T}{1-T} \exp\left(-\frac{\tau}{\tau_{\text{TRIPLET}}} \right) \right] \end{aligned} \quad (2)$$

In Eq. 2, T is the fraction of molecules in the triplet state in the detection volume and τ_{TRIPLET} is the characteristic relaxation time for the single-triplet relaxation (Schwille et al. 2000).

When a constant laminar flow is applied to the sample, the fluctuations of the fluorescence are influenced by the

process of uniform translation of the tracers (Magde et al. 1978). If the transport rate due to laminar flow is small compared to free diffusion, i.e., $\tau_{\text{flow}} \geq \tau_{\text{DIFF}}$, the effect of flow in the $G(\tau)$ curve is less prominent, and it is necessary to take into account both the contributions due to flow and diffusion (Brister et al. 2005; Gosch et al. 2000). The expression for the autocorrelation curve is given by:

$$G(\tau) = \frac{1}{N} \left(1 + \frac{\tau}{\tau_{\text{DIFF}}}\right)^{-1} \left(1 + \frac{\tau}{S^2 \tau_{\text{DIFF}}}\right)^{-1/2} \times \left[1 + \frac{T}{1-T} \exp\left(-\frac{\tau}{\tau_{\text{TRIPLET}}}\right)\right] \times \exp\left\{-\left(\frac{\tau}{\tau_{\text{flow}}}\right)^2 \left(1 + \frac{\tau}{\tau_{\text{DIFF}}}\right)^{-1} \times \left(1 + \frac{\tau}{S^2 \tau_{\text{DIFF}}}\right)^{-1/2}\right\} \quad (3)$$

In the opposite regime, if $\tau_{\text{flow}} \ll \tau_{\text{DIFF}}$, the contribution of diffusion can be neglected with respect to the flow process and the previous expression can be simplified to (Kuricheti et al. 2004b)

$$G(\tau) = \frac{1}{N} \exp\left\{-\left(\frac{\tau}{\tau_{\text{flow}}}\right)^2\right\} \quad (4)$$

Equation 3 is used to fit the autocorrelation curve measured in the microchannel with an external applied flow rate. Since τ_{flow} can be considered as the average transit time of the tracer through the detection volume, the average flow speed v can be calculated as $v = \omega_0/\tau_{\text{flow}}$.

The experimental parameters characterizing the microscope focal volume and the sample, which are the shape factor S , T , τ_{DIFF} , and τ_{TRIPLET} , are determined from initial calibration measurements in the absence of flow in the microchannel. Briefly, the laser beam is focused inside the channel and the brightness of the fluorophore (Alexa488) is maximized through the correction collar adjustment to take into account the coverglass thickness in that position. The FCS curve is then collected and analyzed.

Typically for our experimental set-up and Alexa488 solution at 22°C ($D = 3.9 \times 10^{-10} \text{ m}^2/\text{s}$ (Petrov and Schille 2008; Kestin et al. 1978)), these fitting parameters are: $S = 5.2 \pm 0.5$, $\tau_{\text{DIFF}} = 24 \pm 1 \text{ }\mu\text{s}$, $T = 6 \pm 1\%$ and $\tau_{\text{TRIPLET}} = 3 \pm 0.5 \text{ }\mu\text{s}$. However not all these parameters are really free, since τ_{TRIPLET} can be compared with literature data. These findings show that the half-length dimensions of the detection volume are usually $1 \pm 0.1 \text{ }\mu\text{m}$ in the axial and $0.193 \pm 0.005 \text{ }\mu\text{m}$ in the lateral direction, resulting in a detection volume of less than 1 fl ($\sim 0.2 \text{ fl}$). These dimensions of the focal volume are much smaller than the dimensions of the microchannel, thus guaranteeing a uniform flow measurement within the focal volume.

Parameters S , T , τ_{DIFF} , and τ_{TRIPLET} are then fixed in the fitting procedure of the FCS curves recorded in the presence of the flow at the same position in the channel of the calibration measurement. Just for comparison with other timescales, we obtained from the fitting: $\tau_{\text{flow}} = 19 \pm 1 \text{ }\mu\text{s}$ corresponding to $v_{\text{flow}} = 10 \text{ mm s}^{-1}$. It is therefore necessary in the fitting procedure to consider also the contribution of diffusion.

The error on the velocity value is determined from the propagation error formula, considering the errors on τ_{flow} and τ_{DIFF} from the fitting and the uncertainty affecting the estimate of the diffusion coefficient of the fluorescent dye.

In the same context, from the fit of $G(\tau)$ curves, it is also possible to extract the number of molecules N in the focal volume (Lakowicz 2006). This feature is of extreme importance when the technique is applied to study the hydrodynamic focusing effect, because it gives a quantitative measurement of tracer concentration with high spatial resolution and sensibility. The amplitude of $G(\tau)$ at $\tau = 0$ is inversely proportional to the number of molecules in the detection volume. The average molar concentration of the fluorophores therefore can be evaluated from the relation: $\langle C \rangle = \frac{N}{V_{\text{DET}} N_{\text{Av}}}$, with N_{Av} Avogadro’s number, and V_{DET} is the effective observation volume. The effective volume is dependent on the shape of the detection function. For Gaussian beam, a good approximation is given by: $V_{\text{DET}} = \pi^{3/2} S(\omega_0)^3$.

Some artifacts, inherent to the FCS technique, can indeed cause a wrong determination of the amplitude of the autocorrelation curve. In our experiments, to avoid the artifact due to the detector afterpulsing effect at short times, we use the “pseudo cross-correlation” method (Burstyn and Sengers 1983). By splitting the output signal into two parts and cross-correlating the data collected from two different APDs, it is possible to eliminate this distorting effect. Another source of error can arise from the use of fluorophores with a huge number of molecules in a dark state, such as molecules with high intersystem crossing efficiency, because it is more difficult to consider the effect of blinking with respect to the diffusion contribution. The Alexa488 dye, at low excitation power, is characterized by a triplet quantum yield less than 8% that assures small uncertainties in the calculation of the local concentrations.

The error on the tracer concentration is determined from propagation error formula, considering the errors on N , S and τ_{DIFF} evaluated with the fitting procedure and the uncertainty on the diffusion coefficient of the fluorescent dye.

3.2 Numerical simulations

The steady-state fluid flow and molecular diffusion in the microdevice are simulated using the commercial software

COMSOL 3.5 which allows numerical finite element simulations. The microchannel under consideration has a 3D rectangular shape. The x -axis marks the flow direction and the cross-section of the channel lies in the yz -plane. The y -axis is chosen to define the channel width, whereas the z -axis lies along the channel depth. For the simulations, we consider the same dimensions determined from the experimental measurements on the device depicted in Fig. 1c. The flow velocity field $\mathbf{u} = (u_x, u_y, u_z)^T$ is found by solving the steady state incompressible Navier–Stokes equations:

$$\begin{aligned} \rho u_j \frac{\partial u_i}{\partial r_j} - \mu \nabla^2 u_i + \frac{\partial p}{\partial r_j} &= 0 \\ \frac{\partial u_i}{\partial r_j} &= 0 \end{aligned} \quad (5)$$

with $i, j = x, y, z$; these are coupled to steady convection–diffusion equation for the concentration c of the species

$$u_j \frac{\partial c}{\partial r_j} - D \nabla^2 c = 0 \quad (6)$$

where the parameters are D , the diffusion coefficients of the species; ρ , the fluid density; μ , the dynamic viscosity; and p , the pressure. Values typical of water are assumed. Simulations are carried out using the diffusion coefficient of Alexa488 in water at 22°C to allow a direct comparison with the experimental conditions. The boundary condition at the inlet of the channels is set as velocity-inlet boundary (Bransky et al. 2008). Throughout the whole study, the inlet velocity for the central channel is set as 0.7 mm/s (within the range estimated from the experiments). In this study, the two side channel flow velocities are different (see Table 1 for experimental values). In the simulations, these different flow velocities are taken into account. However a nominal parameter k set equal to 1, 2, and 4 is used to discriminate the three different regimes used for the flow velocities of the sheath fluids with respect the central one. The boundary condition at the outlet is set as a static outlet pressure (Mathur and Murthy 1997) equal to 0. At the inlet (central and lateral channels) the velocity profile is considered as parabolic (for details see Sect. 4). No-slip conditions ($\mathbf{u} = 0$) are applied at the channel walls. Concentrations c are set equal to the experimental data

Table 1 Comparison between experimental velocity values in the three channels at different k regimes

k	Experimental values (mm s ⁻¹)		
	Central CH	Left side CH	Right side CH
1	0.9 ± 0.2	0.8 ± 0.2	1.0 ± 0.2
2	0.9 ± 0.2	1.4 ± 0.1	2.0 ± 0.1
4	0.9 ± 0.2	3.2 ± 0.1	3.9 ± 0.1

concentrations at the inlet central channel, whereas at the inlet of the two side channels it is set to 0.

4 Results and discussion

4.1 Characterization of flow properties inside the micro-channels

The initial characterization of the pressure driven laminar flow properties in the central and sheath channels is conducted injecting directly Alexa488 solution in both inlets to completely fill the device. The velocity profile across the central channel is detected by measuring the FCS curve at different distances from the center of the channel towards the lateral walls. Each FCS curve is fitted using Eq. 3, with S , T , τ_{DIFF} and τ_{TRIPLET} fixed from the preliminary calibration in the same positions without flow. These preliminary measurements are aimed at a careful characterization of the experimental conditions that, if not properly accounted for, can be source of artifacts. Examples of such conditions are: the deformation of the focal volume or the number of molecules in the larger detection volume approaching the PDMS lateral wall.

In Fig. 2, the velocity profile measured in the y (square) and z (dots) directions of the central channel are reported, together with the trend predicted from numerical simulations (solid lines). In both cases, the flow rate in the syringe pump is set at 1 $\mu\text{l}/\text{min}$. These profiles deviate from the parabolic dependence on the channel dimensions as a consequence of its rectangular shape (Kunst et al. 2002). Since the fluid is injected by a cylindrical tube where the velocity profile is parabolic, in the numerical simulations we choose a parabolic profile at the beginning of the

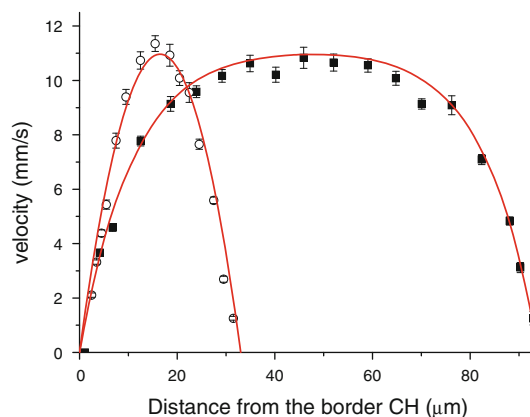


Fig. 2 Flow profiles measured with FCS experiment in the y (square) and z (dots) directions as a function of the distance from the border of the channel. The solid lines are the results of numerical simulations of flow profiles

rectangular channel. The good agreement confirms nevertheless the choice of initial conditions that are adopted throughout all the simulations. It is useful to point out that the shapes of the profiles are independent from the applied flow rate and therefore it is possible to linearly rescale the curves with the applied injection flow speed. As expected, the maximum velocity is reached in the center of the channel along the y and z direction.

The velocities at the center of the channel are also measured in each arm of the sheath channels. The measured velocities are reported in Table 1. The data are the average of five measurements and the errors are calculated as half the difference between the maximum and the minimum values. The large uncertainty for the lowest speed value takes into account the difficulty in separating the flow term with respect to the diffusion contribution in the FCS data.

The fluxes from the side channels are not symmetrical: the fluid velocity from the right side channel is at least 20% higher than the flux from the left side channel.

4.2 Hydrodynamic focusing characterization and comparison with 3D simulation data

The hydrodynamic focusing process is characterized by observing the behavior of the fluorescent dye Alexa488 injected only in the central channel, and applying to the side channels a flow velocity equal or higher than the one in the central line. The direct visualization of this effect is observed simply by mapping the fluorescence signal in the microchannel through the confocal microscope, whereas FCS measurements give more quantitative data on the output stream characteristics.

Simulations are carried out at different k regimes with the lateral and the central flow rates computed according to the experimental values reported in Table 1. The images of hydrodynamic focusing of Alexa488 and the simulated results, for the three different k values at the center of the channel along z direction, are shown in Fig. 3. The upper half of each panel shows the experimental CLSM image of the channel: the Alexa488 dye solution (green in the image) comes from the central inlet and, as expected, it is focalized in the central part of the output channel. The lower half panels show the three-dimensional simulation results. In Fig. 3a, b, and c, the experimental and simulations results for $k = 1, 2$, and 4 are reported. The agreement between the experimental and simulated images is very good, as the measured asymmetric flow patterns caused by different values of the flow rate in the two side channels are well reproduced. This is particularly evident when k is large (Fig. 3c). As measured, the larger value of the velocity in the right side channel with respect to the left one determines the strong asymmetry of the central flux.

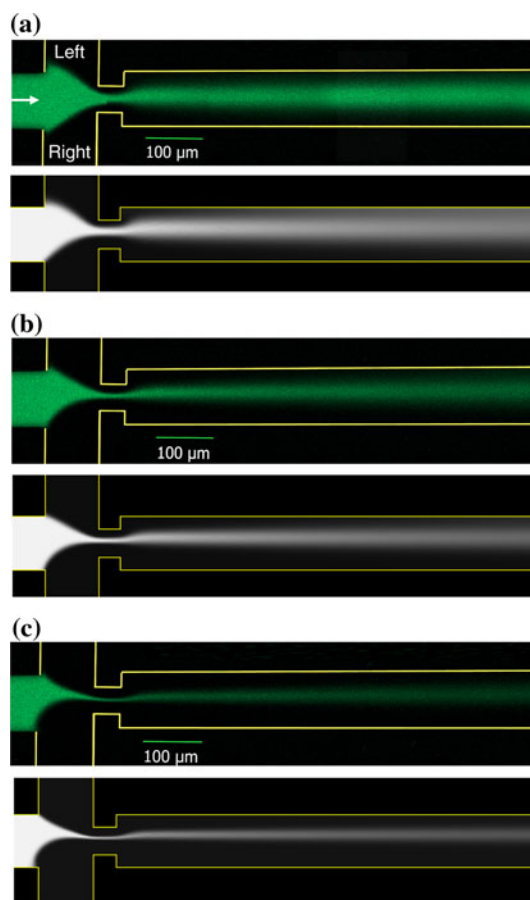


Fig. 3 Comparison between the experimental (*upper part*) and simulated (*lower part*) concentration along the channel for different k . **a** $k = 1$, **b** $k = 2$ and **c** $k = 4$

The flow velocity on the right side is so large with respect to the left one that the right flow partially enters in the left part of the central channel and causes an asymmetric position of the focused flux along the whole central channel. This experimental behavior is reproduced in details by the simulation results. Figure 3 gives a pictorial representation of the distribution of the fluorescent dye in the nearby of the cross-like junction. Quantitative results are reported in Fig. 4, showing the experimental and simulated (solid line) concentration profiles of Alexa488 along the central channel. The experimental concentration data are extrapolated from Eq. 3 employed to fit the FCS curves. Agreement between simulations and experimental data at the two lowest k values is satisfactory, while at higher k values the comparison is less favorable. At this ratio, the simulated concentration values appears to be slightly shifted along the x -position with respect to the experimental finding, although this shift can be justified by the measurements conditions, characterized by a very thin focused flux in the bottleneck region of $5 \mu\text{m}$. It is therefore more difficult to focus the laser beam in the central

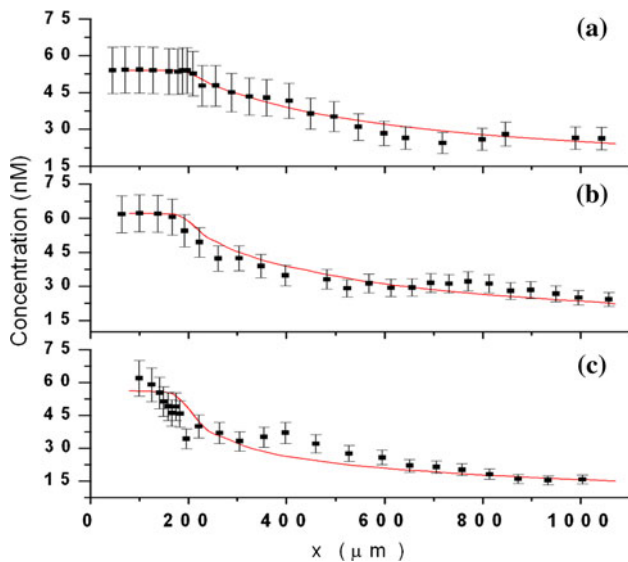


Fig. 4 Comparison between the experimental (*scattered line*) and simulated (*solid line*) data of fluorescent tracer concentration profile along the central channel for different k . **a** $k = 1$, **b** $k = 2$ and **c** $k = 4$

part of the stream. Small drifts in the position of the focused stream, due most probably to the syringe pump injection system or, to a minor degree, to the mounting stage of the microscope, can move the excitation focus partially outside the central flow and reduce the reliability of the experimental values from the fitting of FCS curves. The concentration error bars are large because of the significant error affecting the confocal shape factor evaluated from the initial fitting without laminar flow.

Next, we compare in detail experimental and simulated data for $k = 2$. Similar considerations can be done for $k = 1$ and 4. We discuss first the flow characteristics and then the concentration profile of the fluorescent dye in the focused flow. Figure 5 shows the fluid velocities from the FCS measurements carried out along the x -direction in the center of the focused flow. The y -position of the focused flow along the central channel does not lie in the middle of the channel itself, because of the different velocity values for the sheath flows in the lateral channels. The experimental points are measured in the center of the stream (along the y direction) moving along the focused stream. The peak is the result of the bottleneck after the cross-junction. The raise of the flow speed before and after the junction at the bottleneck is approximately proportional to the increase of the ratio between velocities. The solid line in Fig. 5 shows the simulated data obtained changing the check position along the x -axis to follow the experimental measurements. The dotted line represents the simulation data for a microfluidic device without the bottleneck in the circuit geometry. This behavior is in accordance with a similar microfluidic device described by Hertzog et al. (2006).

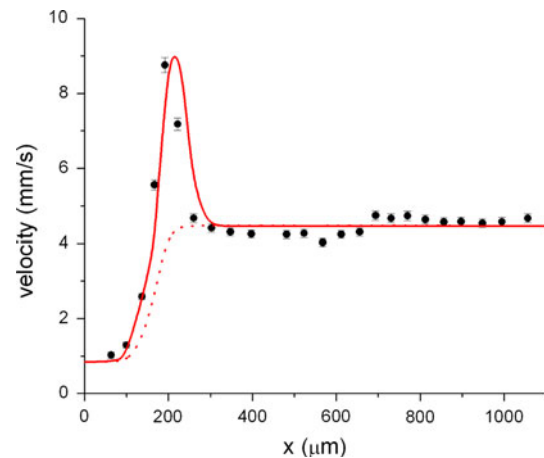


Fig. 5 Simulated (*solid line*) and experimental (*scattered line*) data of the velocity field along the central channel for $k = 2$. The *dotted line* is the simulation data for the same device but without the bottleneck

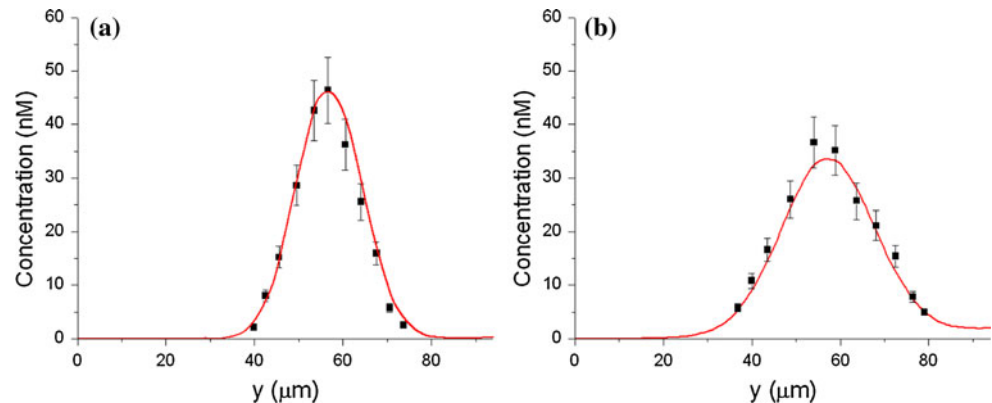
Due to the focusing effect, the concentration of the fluorescent tracer Alexa488, in the cross-section of the zy -plane, peaks in the central region of the channel and decreases towards zero at the channel walls. The concentration profiles in the zy -plane of Alexa488 along the x -axis are influenced by both the diffusion component and the convective component of the tracer molecule motion. Due to these two influences, the tracer moves in the transverse direction causing a widening of the concentration profile as the x -value increases. To quantify this behavior, we define the full-width at half-maximum (FWHM) of the concentration profile in the y -direction as the width that corresponds to the locations where the concentration falls at half of its maximum value.

The numerical evaluation of the focused stream FWHM with and without the bottleneck can be used as a direct test of the mixing enhancement in this particular device geometry. For the $k = 2$ case, for example, and at $x = 215 \mu\text{m}$ (corresponding to the center of the bottleneck, see Fig. 1c), the FWHM of the concentration profile is 7.8 and 14.6 μm with and without the bottleneck, respectively. The reduction of the FWHM is related to a decrease of the mixing time, since the average time of a molecule to diffuse over a distance is proportional with the square of the distance (Zhang et al. 2008).

In Table 2, we report the position of the maximum value (*Position* column) and the FWHM of the concentration profile at two different transversal sections along the central channel equal to 285 and 515 μm with respect to the $x = 0$ point (see Fig. 1c). At 285 μm , the focused flux has just flowed through the bottleneck whereas at the second section the flux is stabilized along the channel. At low k regimes, it is more difficult to observe a well-focused flux

Table 2 Comparison between experimental and the simulated values for the position of the maximum value (*position* column) and the FWHM (see text) of the concentration profile of the fluorescent tracer in two transversal sections of the channel

<i>k</i>	Experimental values (μm)				Simulated values (μm)			
	285 μm		515 μm		285 μm		515 μm	
	Position	Width	Position	Width	Position	Width	Position	Width
1	53.0	31.1	55.2	34.8	53.4	26.1	54.0	34.5
2	56.5	17.8	56.9	25.7	56.7	17.9	57.1	25.1
4	56.9	11.3	56.8	17.6	56.2	11.5	56.7	16.6

Fig. 6 Experimental (*scattered line*) and simulated (*solid line*) transversal concentration profiles at **a** 285 μm and **b** 515 μm . All the profiles are measured for *k* equal to 2

along the 1,000 μm channel, due to the increased flow velocity, as shown by the spread of the Alexa488 dye in Fig. 3 towards the walls of the channel and in particular, given the asymmetric sheath flow, along the left wall. Figure 6a and b show the comparison between the experimental (symbol) and simulated (solid line) data for the concentration at 285 and 515 μm , respectively. The concentration profile in Fig. 6a assumes a Gaussian shape, whereas the concentration profile in Fig. 6b loses partially the symmetric shape, because of the influence of the diffusion effects. This behavior is more evident at low *k* regimes, while the concentration profile at high *k* regimes maintains the original shape. The agreement between experimental and simulated data is very good, and the observed spreading of the central flow in the experimental device is reproduced accurately.

5 Conclusions

In this work, an integrated analysis of an asymmetric flux of a fluorescent dye in a microfluidic device has been carried out combining FCS and hydrodynamic modeling. In particular, a microfluidic device exploiting the focusing effect has been observed in the presence of Alexa488, subject to an asymmetric focused flow. The direct observation of the flowing fluid has been carried out using fluorescence correlation spectroscopy, which allows a

direct measure of the flow rates in the channels and the variation of the species concentration in correspondence of the central focused flux. Modeling has been based on a standard Navier–Stokes finite-element approach, coupled to convection–diffusion equations for the fluorescent solute. Numerical simulations reproduce in details the shape, the position, and the width of the velocity and concentration profiles along the central channel and along the transversal and vertical sections of the microfluidic device.

Acknowledgments The authors gratefully acknowledge Eugene Petrov, Markus Burkhardt, and Wolfgang Staroske for helpful discussions and advices. Fondazione CARIPARO (MISCHA project, call 2007) and University of Padova PRAT (2007) are gratefully acknowledged for financial support.

References

- Bransky A, Korin N, Levenberg S (2008) Experimental and theoretical study of selective protein deposition using focused micro laminar flows. *Biomed Microdevice* 10:421–428
- Brister PC, Kuricheti KK, Buschmann V, Weston KD (2005) Fluorescence correlation spectroscopy for flow rate imaging and monitoring—optimization, limitations and artifacts. *Lab Chip* 5:785–791
- Brody JP, Yager P, Goldstein RE, Austin RH (1996) Biotechnology at low Reynolds numbers. *Biophys J* 71:3430–3441
- Burstyn HC, Sengers JV (1983) Time dependence of critical concentration fluctuations in a binary liquid. *Phys Rev A* 27:1071–1085

- Chang CC, Huang ZX, Yang RY (2007) Three-dimensional hydrodynamic focusing in two-layer polydimethylsiloxane (PDMS) microchannels. *J Micromech Microeng* 17:1479–1486
- Chen CH, Cho SH, Tsai F, Erten A, Lo YH (2009) Microfluidic cell sorter with integrated piezoelectric actuator. *Biomed Microdevices* 11:1223–1231
- Chung S, Park SJ, Kim JK, Chung C, Han DC, Chang JK (2003) Plastic microchip flow cytometer based on 2- and 3-dimensional hydrodynamic flow focusing. *Microsystem Technol* 9:525–533
- Criswell KA, Bleavins MR, Zielinski D, Zandee JC, Walsh KM (1998) Flow cytometric evaluation of bone marrow differentials in rats with pharmacologically induced hematologic abnormalities. *Cytometry* 32:18–27
- Cubaud T, Mason TG (2008) Formation of miscible fluid microstructures by hydrodynamic focusing in plane geometries. *Phys Rev E* 78:056308
- Darnton N, Bakajin O, Huang R, North B, Tegenfeldt JO, Cox EC, Sturm J, Austin RH (2001) Hydrodynamics in 2½ dimensions: making jets in a plane. *J Phys* 13:4891–4902
- Deshpande A, Gua Y, Matthews S, Yunusa K, Slaterna N, Brennanb C, Fishera A (2009) Hydrodynamic focusing studies in microreactors using voltammetric analysis: theory and experiment. *Chem Eng J* 49:428–434
- Dittrich PS, Schwille P (2002) Spatial two-photon fluorescence cross-correlation spectroscopy for controlling molecular transport in microfluidic structures. *Anal Chem* 74:4472–4479
- Dittrich PS, Schwille P (2003) An integrated microfluidic system for reaction, high-sensitivity detection, and sorting of fluorescent cells and particles. *Anal Chem* 75:5767–5774
- Domagalski PM, Mielnik MM, Lunde I, Sætran LR (2007) Characteristics of hydrodynamically focused streams for use in microscale particle image velocimetry (Micro-PIV). *Heat Transf Eng* 28:680–687
- Egawa T, Durand JL, Hayden EY, Rousseau DL, Yeh SR (2009) Design and evaluation of a passive alcove-based microfluidic mixer. *Anal Chem* 81:1622–1627
- Elson EL, Magde D (1974) Fluorescence correlation spectroscopy I. Conceptual basics and theory. *Biopolymers* 13:1–27
- Fenili D, Pirovano B (1998) The automation of sediment analysis using a new urine flow cytometer. *Clin Chem Lab Med* 36:909–917
- Ghosh M, Alves C, Tong Z, Tettey K, Konstantopoulos K, Stebe KJ (2008) Multifunctional surfaces with discrete functionalized regions for biological applications. *Langmuir* 24:8124–8142
- Gosch M, Blom H, Holm J, Heino T, Rigler R (2000) Hydrodynamic flow profiling in microchannel structures by single molecule fluorescence correlation spectroscopy. *Anal Chem* 72:3260–3265
- Hertzog DE, Ivorra B, Mohammadi B, Bakajin O, Santiago JC (2006) Optimization of a microfluidic mixer for studying protein folding kinetics. *Anal Chem* 78:4299–4306
- Kestin J, Sokolov M, Wakeham WA (1978) Viscosity of liquid water in the range -8°C to 150°C . *J Phys Chem Ref Data* 7:941–948
- Kim YR, Yee M, Metha S, Chupp V, Kendall R, Scott CS (1998) Simultaneous differentiation and quantitation of erythroblasts and white blood cells on a high throughput clinical haematology analyzer. *Clin Lab Haematol* 20:21–29
- Kohlheyer D, Besselink GAJ, Schlautmann S, Schasfoort BM (2006) Free-flow zone electrophoresis and isoelectric focusing using a microfabricated glass device with ion permeable membranes. *Lab Chip* 6:374–380
- Kunst BH, Schots A, Visser AJWG (2002) Detection of flowing fluorescent particles in a microcapillary using fluorescence correlation spectroscopy. *Anal Chem* 74:5350–5357
- Kuricheti KK, Buschmann V, Weston KD (2004a) Application of fluorescence correlation spectroscopy for velocity imaging in microfluidic devices. *Appl Spectrosc* 58:1180–1186
- Kuricheti KK, Buschmann V, Brister P, Weston KD (2004b) Velocity imaging in microfluidic devices using fluorescence correlation spectroscopy. *Microfluidics, BioMEMS, and medical microsystems II*. Proc SPIE 5345:194–205
- Lakowicz JR (2006) Principles of fluorescence, Chap 24, 3rd ed. Springer, New York
- Larsen MU, Shapley NC (2007) Stream spreading in multilayer microfluidic flows of suspensions. *Anal Chem* 79:1947–1953
- Lee GB, Hung CI, Ke BJ, Huang GR, Hwei RH, Lai HF (2001a) Free-flow zone electrophoresis and isoelectric focusing using a microfabricated glass device with ion permeable membranes. *Trans ASME Chem* 123:672–679
- Lee GB, Hwei BH, Huang GR (2001b) Micromachined pre-focused $M \times N$ flow switches for continuous multi-sample injection. *J Micromech Microeng* 11:654–661
- Lee GB, Chang CC, Huang SB, Yang RJ (2006) The hydrodynamic focusing effect inside rectangular microchannels. *J Micromech Microeng* 16:1024–1032
- Lin CC, Chen A, Lin CH (2008) Microfluidic cell counter/sorter utilizing multiple particle tracing technique and optically switching approach. *Biomed Microdevices* 10:55–63
- Liu C, Stakenborg T, Peeters S, Lagae L (2009) Cell manipulation with magnetic particles toward microfluidic cytometry. *J Appl Phys* 105:102014-1–102014-11
- Magde D, Webb W, Elson E (1978) Fluorescence correlation spectroscopy III. Uniform translation and laminar flow. *Biopolymers* 17:361–376
- Mark D, Haeberle S, Roth G, von Stetten F, Zengerle R (2010) Microfluidic lab-on-a-chip platforms: requirements, characteristics and applications. *Chem Soc Rev* 39:1153–1182
- Mathur SR, Murthy JY (1997) Pressure boundary conditions for incompressible flow using unstructured meshes. *Numer Heat Transf B* 32:283–298
- Nguyen NT, Huang X (2005) Mixing in microchannels based on hydrodynamic focusing and time-interleaved segmentation: modelling and experiment. *Lab Chip* 5:1320–1326
- Nguyen NT, Yap YF, Sumargo A (2008) Microfluidic rheometer based on hydrodynamic focusing. *Meas Sci Technol* 19:085405-1–085405-9
- Pamme N, Wilhelm C (2006) Continuous sorting of magnetic cells via on-chip free-flow magnetophoresis. *Lab Chip* 6:974–980
- Park HY, Qiu X, Rhoades E, Koralach J, Kwok LW, Zipfel WR, Webb WW, Pollack L (2006) Achieving uniform mixing in a microfluidic device: hydrodynamic focusing prior to mixing. *Anal Chem* 78:4465–4473
- Petrov EP, Schwille P (2008) Standardization and quality assurance in fluorescence measurements II: bioanalytical and biomedical applications. Springer series on fluorescence, vol 6, pp 145–197
- Ren L, Sinton D, Li D (2003) Numerical simulation of microfluidic injection processes in crossing microchannels. *J Micromech Microeng* 13:739–747
- Schwille P, Kummer S, Heikal AA, Moerner WE, Webb WW (2000) Fluorescence correlation spectroscopy reveals fast optical excitation-driven intramolecular dynamics of yellow fluorescent proteins. *Proc Natl Acad Sci USA* 97:151–156
- Simonnet C, Groisman A (2005) Two-dimensional hydrodynamic focusing in a simple microfluidic device. *Appl Phys Lett* 87:114104-1–114104-3
- Sinton D (2004) Microscale flow visualization. *Microfluid Nanofluid* 1:2–21
- Song C, Nguyen NT, Tan SH, Asundi AK (2009) Modelling and optimization of micro optofluidic lenses. *Lab Chip* 9:1178–1184
- Srisa-Art M, Bonzani IC, Williams A, Stevens MM, de Mello AJ, Edel JB (2009) Identification of rare progenitor cells from human periosteal tissue using droplet microfluidics. *Analyst* 134:2239–2245

- Wang F, Wang H, Wang J, Wang HY, Rummel PL, Garimella SV, Lu C (2008) Microfluidic delivery of small molecules into mammalian cells based on hydrodynamic focusing. *Biotechnol Bioeng* 100:150–158
- Wereley ST, Meinhart CD (2010) Recent advances in micro-particle image velocimetry. *Ann Rev Fluid Mech* 42:557–576
- Wong PK, Lee YK, Ho CM (2003) Deformation of DNA molecules by hydrodynamic focusing. *J Fluid Mech* 497:55–65
- Wu Z, Nguyen NT (2005) Hydrodynamic focusing in microchannels under consideration of diffusive dispersion: theories and experiments. *Sens Actuators B* 107:965–974
- Xuan X, Li D (2005) Focused electrophoretic motion and selected electrokinetic dispensing of particles and cells in cross-microchannels. *Electrophoresis* 26:3552–3560
- Yamada M, Seki M (2006) Microfluidic particle sorter employing flow splitting and recombining. *Anal Chem* 78:1357–1362
- Yang AS, Hsieh WH (2007) Hydrodynamic focusing investigation in a micro-flow cytometer. *Biomed Microdev* 9:113–122
- Yeh HC, Puleo CM, Lim TC, Ho YP, Giza PE, Huang RC, Wang TH (2006) A Microfluidic-FCS platform for investigation on the dissociation of Sp1-DNA complex by doxorubicin. *Nucl Acids Res* 34:e144
- Zhang Z, Zhao P, Xiao G, Lin M, Cao X (2008) Focusing-enhanced mixing in microfluidic channels. *Biomicrofluidics* 2:014101